Scalable joint segmentation and registration framework for infant brain images

Pei Dong[a], Li Wang[a], Weili Lin[a], Dinggang Shen[a,b,*], Guorong Wu[a,**]

[a] *Department of Radiology and BRIC, University of North Carolina at Chapel Hill, NC 27599, USA*
[b] *Department of Brain and Cognitive Engineering, Korea University, Seoul 02841, Republic of Korea*

ABSTRACT

The first year of life is the most dynamic and perhaps the most critical phase of postnatal brain development. The ability to accurately measure structure changes is critical in early brain development study, which highly relies on the performances of image segmentation and registration techniques. However, either infant image segmentation or registration, if deployed independently, encounters much more challenges than segmentation/registration of adult brains due to dynamic appearance change with rapid brain development. In fact, image segmentation and registration of infant images can assists each other to overcome the above challenges by using the growth trajectories (i.e., temporal correspondences) learned from a large set of training subjects with complete longitudinal data. Specifically, a one-year-old image with ground-truth tissue segmentation can be first set as the reference domain. Then, to register the infant image of a new subject at earlier age, we can estimate its tissue probability maps, i.e., with sparse patch-based multi-atlas label fusion technique, where only the training images at the respective age are considered as atlases since they have similar image appearance. Next, these probability maps can be fused as a good initialization to guide the level set segmentation. Thus, image registration between the new infant image and the reference image is free of difficulty of appearance changes, by establishing correspondences upon the reasonably segmented images. Importantly, the segmentation of new infant image can be further enhanced by propagating the much more reliable label fusion heuristics at the reference domain to the corresponding location of the new infant image via the learned growth trajectories, which brings image segmentation and registration to assist each other. It is worth noting that our joint segmentation and registration framework is also flexible to handle the registration of any two infant images even with significant age gap in the first year of life, by linking their joint segmentation and registration through the reference domain. Thus, our proposed joint segmentation and registration method is scalable to various registration tasks in early brain development studies. Promising segmentation and registration results have been achieved for infant brain MR images aged from 2-week-old to 1-year-old, indicating the applicability of our method in early brain development study.

1. Introduction

Human brain undergoes rapid physical growth and functional development from birth to 1-year-old [1–4]. The ability to accurately measure structural brain changes from MR (Magnetic Resonance) images at this period is indispensable for shedding new light on the exploration of brain development and also the early detection of neurodevelopmental disorder. For example, infants with autism were found to have 5–10% abnormal enlargement in total brain volume at early development stage [5,6].

However, the automatic image segmentation and registration tools for processing a large amount of infant brain MR images lag behind the demands of ongoing neuroscience and clinical studies. In particular, image segmentation [7–11] and registration [12,13], which are the two most essential steps, are largely needed in many early brain development studies, such as longitudinal cortical analysis [14,15] and infant atlas construction [16]. Recent patch based label fusion methods, such as local weighted label fusion method [17], non-local mean label fusion method [18], and sparse learning based label fusion methods [9–11,19–21], have been successfully applied to medical image segmentations. However, these methods fail to achieve their expected performance when applying to the infant brain segmentation. Both infant
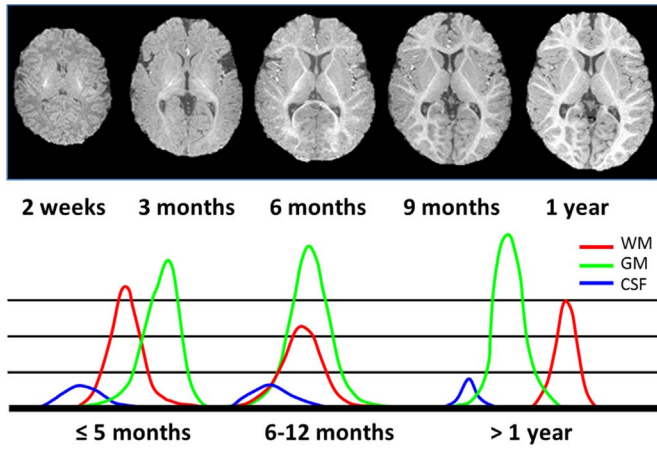
Fig. 1. Dynamic appearance and anatomical changes on a typical infant brain from 2-week to 1-year old.

image segmentation and registration are challenged by:

(1) The dynamic appearance changes of brain tissues from birth to 1-year-old [1]. Due to myelination of WM (white matter), the intensity characteristics change dramatically in different development stages, as shown by the intensity histograms of WM, GM (gray matter), and CSF (cerebral-spinal fluid) in Fig. 1. Specially, at the age around 3-6 months, the contrast between WM and GM is very small. This poses challenges for both identifying tissues in segmentation and establishing correspondences in registration.

(2) The fast and spatially-varied developments of brain anatomy and size. Brain development in the first year of life is extremely fast, with different structures having different growth patterns [22]. For example, the majority of hemispheric growth is accounted for by GM which increases 149% in the first year, while the hemispheric WM volume increases by only 11%. Consequently, either segmentation or registration, if deployed independently, is difficult to handle the above challenges.

Since the imaging-based study on early brain development becomes more and more popular, a sufficient number of longitudinal infant brain images have been collected in UNC at Chapel Hill in the past years. Many subjects with complete longitudinal images (at 2 weeks, 3 months, 6 months, 9 months, and 1 year of age) have been well segmented by either human interactions or automatic methods with multi-modality information (T1, T2 and DTI) [23–25]. As demonstrated by many literatures, appropriate joint segmentation and registration could significantly improve both of their performances [26–30]. To this end, we propose a novel joint segmentation and registration framework to simultaneously segment brain tissues and also estimate the deformation pathway between any pair of infant brain images from the same subject or different subjects. The leverage to achieve the success of this project is a large number of infant images already acquired. It is worth noting that these valuable results are often ignored when performing segmentation or registration for the infant subjects with incomplete or even no longitudinal follow-up data. Specifically, we first establish accurate temporal correspondences for any training subject with full longitudinal data in our database, to learn subject-specific growth trajectories [31–33]. Then, a 1-year-old image (with accurate tissue segmentation) is selected as the reference image. To deal with the potential large age gap between two infant images, we will first segment the new infant image with a sparse patch-based level-set technique [34] that allows each patch in the new infant image to look for similar patches in the respective training subjects with similar age and further combines the tissue labels of matched patches in the training subjects to provide good initialization for the level-set seg-

mentation. Based on those matched patches in the training subjects as well as their existing longitudinal growth trajectories, we can also immediately predict the initial deformation pathway between these two new infant brain images. Afterwards, deformations between two new infant images can be refined by the conventional deformable registration upon their segmented images. The refined registration will allow the propagation of reliable label fusion heuristics from the reference image to refine the segmentation of new infant image, which brings the image segmentation and registration to assist each other. By repeating these steps, we can iteratively refine both segmentation and registration of the two new infant images. The advantages of our method include: **(1)** avoiding direct correspondence detection between two infant images with dynamic appearance change and **(2)** improving the performance of image segmentation and registration simultaneously by fully utilizing existing knowledge.

Furthermore, our joint segmentation and registration framework is flexible to extend to the segmentation and registration of any pair of new infant images even with significant age gap in the first year of life. The leverage is registering the infant images at an arbitrary time to the 1-year-old reference image (with good image contrast) using our proposed joint segmentation and registration method. After that, we obtain the deformation pathway between two new infant images by concatenating two deformation pathways, each of which is from particular new infant image to the 1-year-old reference image. Thus, our method is very scalable to deal with various registration tasks in early brain development studies.

We have comprehensively evaluated the segmentation and registration performance for infant images at 2-week-old, 3-month-old, 6-month-old, 9-month-old, and 1-year-old. Specifically, we evaluate the segmentation results with comparison to recently-proposed multi-atlas patch-based approach [34]. In evaluating the registration result, we compare our proposed method to the state-of-the-art deformable image registration methods, including demons registration method [35] (http://www.insight-journal.org/browse/publication/154), the SyN registration method in ANTs package (http://sourceforge.net/projects/advants/) using mutual information [36,37] and cross correlation [38,39] as similarity metric, 3D-HAMMER [40] using the segmented images obtained with iBEAT software (http://www.nitrc.org/projects/ibeat/) [41], and our recently proposed learning-based infant image registration method [42]. Through quantitative measurements and visual inspection, our proposed joint segmentation and registration method achieves the highest accuracy in terms of tissue segmentation and registration.

The remaining parts of this paper are organized as follows. In Section 2, we present our joint segmentation and registration method. In Section 3, we outline the performed experiments and their results. Finally, we draw a conclusion in Section 4.

2. Method

Our goal here is to align an individual infant brain image M_{t_1} with an infant template image F_{t_2}, where t_1 and t_2 are two different ages, each of which could be as young as 2-week-old or as old as 1-year-old. Assume that we have N training subjects I^s ($s = 1, …, N$) with longitudinal data across multiple time points $I^s = \{I_t^s \mid t=1, …, T_s\}$. For each image sequence I^s, we can apply state-of-the-art 4D segmentation method [23,24] to segment 3D image at each time-point into WM (white matter), GM (gray matter), and CSF (cerebral-spinal fluid), which can be denoted as $L^s = \{L_t^s \mid t=1, …, T_s\}$. With some human visual assessment, we can regard these segmentation results of longitudinal training images as the ground truth.

The overview of our proposed joint segmentation and registration method is provided in Fig. 2, which includes both the training and testing stages. In the training stage, we estimate the growth trajectories (Section 2.1) to determine temporal correspondences for each point in the longitudinal data I^s, as delineated by the red dash curves in Fig. 2.
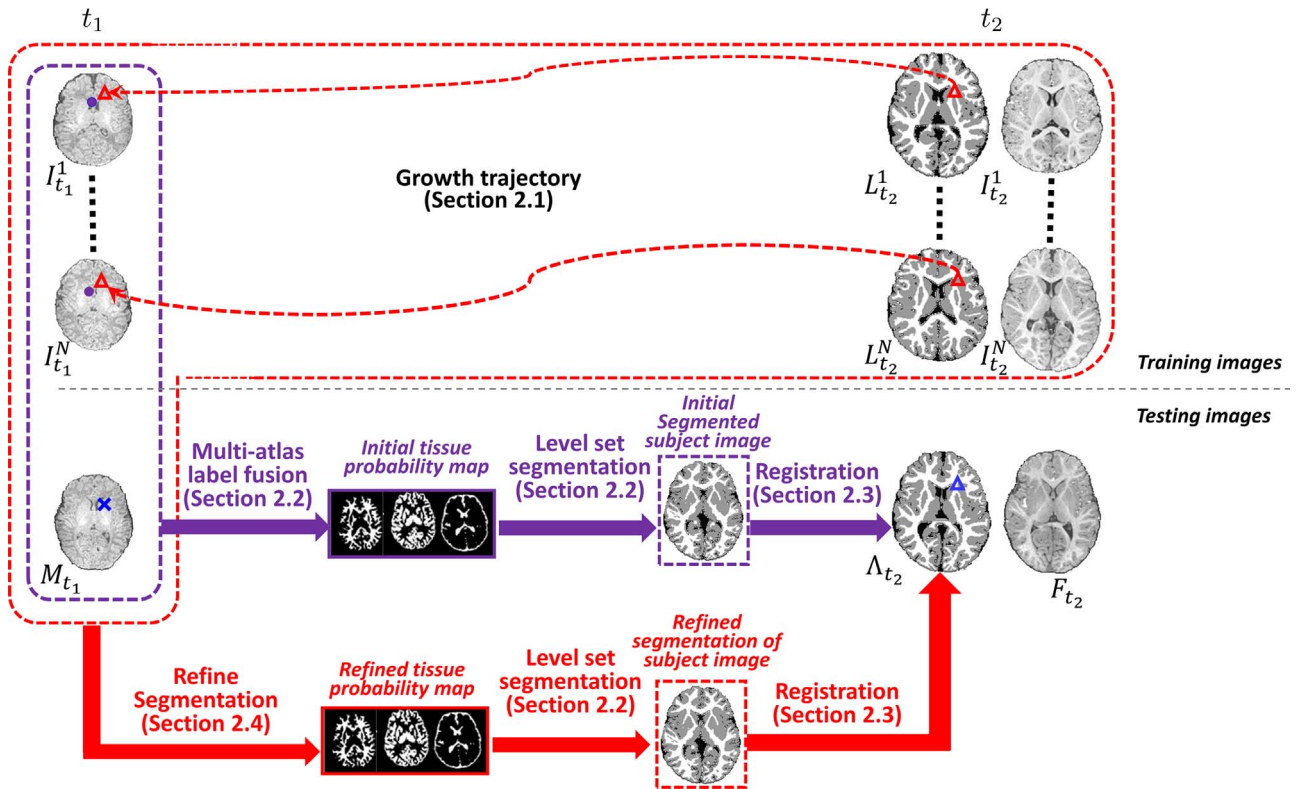
Fig. 2. The overview of our proposed method. (For interpretation of the references to color in this figure, the reader is referred to the web version of this article.)

It is worth noting that here we use F_{t_2}, an individual 1-year-old infant image, as a template image for two reasons: **(1)** it is much easier to segment infant images after one year old since their image appearance looks like adult brain. Thus, the segmentation results in the 1-year-old can be used to guide the segmentation of infant images M_{t_1} at earlier time points [25,43,44], by registering M_{t_1} to F_{t_2}. **(2)** In most brain development studies, 1-year-old brain image is usually used as template. Thus, setting F_{t_2} at 1-year-old as the template image does not significantly compromise the applicability of our proposed joint segmentation and registration method. Actually, it is straightforward to apply our method to simultaneously segment and register any pair of new infant images at the first year of life even with possible large age gap. We will provide the respective solution in Section 2.5. Furthermore, it is reasonable to assume that the 1-year-old template has been accurately segmented into WM, GM, and CSF, denoted by Λ_{t_2}.

To register new infant image to the pre-selected template image F_{t_2} in the testing stage, we can first use sparse patch-based label fusion method [34] to calculate the tissue probability maps for the new infant image M_{t_1} by using only the training images at the similar time-point. Specifically, the label fusion on M_{t_1} selects only the image patches from training images $\{I_{t_1}^s \mid s=1, \ldots, N\}$ at time-point t_1 (as shown in the dash purple box of Fig. 2) to form the patch dictionary. The obtained tissue probability maps can be used as a good initialization for level-set approach for tissue segmentation (Section 2.2). In this way, we can just register the two segmented images, thus avoiding the difficulty of directly registering the original two images with different appearances (Section 2.3). Given the spatial correspondences between M_{t_1} and F_{t_2}, we can further improve the segmentation accuracy of M_{t_1} by incorporating additional label fusion priors from the t_2 time domain at each pair of corresponding locations (blue '×' and 'Δ' in Fig. 2) which are established by image registration (Section 2.4). By alternating these segmentation and registration steps, we can iteratively refine both segmentation and registration results for M_{t_1}.

2.1. Estimating subject-specific growth trajectories

For each training subject with complete longitudinal intensity images I^s and segmentations L^s, a conventional way is to independently register all follow-up images to the baseline image (first time-point). However, such independent image registration may tear down the coherence of temporal correspondences in each longitudinal data. Hence, we go one step further to apply a 4D image registration method [45,46] to simultaneously align images at all time points to its group-mean image G_s. In particular, our registration method has two steps. In Step (1), we hierarchically select a set of key points (red points in Fig. 3) to represent the shape of group-mean image G_s and then establish their correspondences w.r.t. the key points detected in each I_t^s (green points in the top of Fig. 3) by robust feature matching [47]. Meanwhile, by mapping the group-mean image onto the image domain of each time point, every key point in the group-mean shape has several warped points in different time-point images, which can be assembled into a time sequence to form a virtual temporal trajectory (blue dash curves in Fig. 3). Therefore, the temporal coherence in longitudinal infant brain image sequence can be assured by requiring the continuity along all these temporal trajectories. Then, given the correspondences on key points of group-mean image, we can use thin-plate spline (TPS) [48,49] to interpolate the dense deformation fields $\Psi^s = \{\psi_t^s \mid t = 1, \ldots T_s\}$, which will eventually bring each image I_t^s to the common space. In Step (2), we update group-mean image by warping all time-points images I_t^s to the common space and averaging them [50]. These two steps can be repeated until convergence. To obtain the temporal correspondences $\varphi_{t \to t'}^s$ from time points t to t' in the image sequence I^s, we can compose the reverse deformation field $(\psi_t^s)^{-1}$ (from I_t^s to group-mean image) and the forward deformation field $\psi_{t'}^s$ (from group-mean image to $I_{t'}^s$) as $\varphi_{t \to t'}^s = (\psi_t^s)^{-1} \circ \psi_{t'}^s$, where $\circ$ denotes the composition of two deformation pathways [51]. Note, $\varphi_{t \to t'}^s$ is regarded as the growth trajectory of subject image sequence I^s, which can be used to initialize the deformation pathway between the two images F_{t_1} and M_{t_2} (Section 2.3) and iteratively refine the previous segmentation results with the
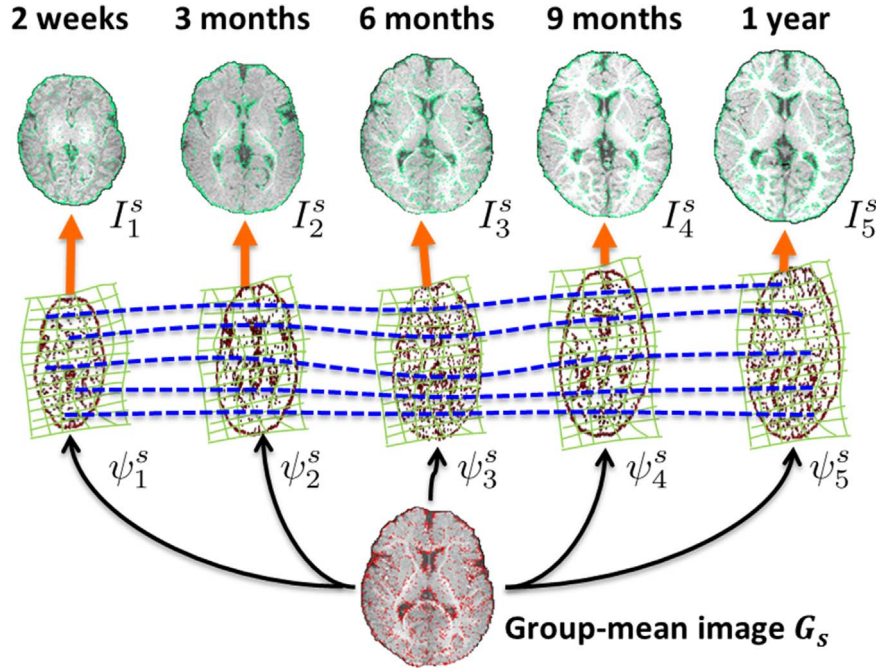
Fig. 3. Estimating the coherent temporal correspondences in an infant image sequence. (For interpretation of the references to color in this figure, the reader is referred to the web version of this article.)

augmented patch dictionary derived from the latest established correspondences (Section 2.4).

2.2. Sparse patch-based level set segmentation

2.2.1. Estimation of tissue probability maps by sparse patch-based label fusion

The initial tissue probability maps for each new infant image are very important to initialize the level set approach for achieving accurate tissue segmentation. Here, we use a sparse patch-based label fusion method [21] to estimate the tissue probability maps for new infant image M_{t_1} by considering the training images with similar age as the atlases.

Specifically, we consider all training images at t_1 time-point, $\{(I_{t_1}^s, L_{t_1}^s) | s = 1, \ldots, N\}$, as the atlases. We first linearly register all atlases to M_{t_1} and then apply deformable registration method to deform all atlases to M_{t_1} image space. To determine the tissue type (WM, GM, or CSF) for each image point x in M_{t_1}, we extract a referent patch $Q(M_{t_1}(x)) \subset M_{t_1}$ centered at image point x. Next, we collect a number of atlas patches $P(I_{t_1}^s(v)) \subset I_{t_1}^s$ across all training infant images $I_{t_1}^s$ at the same time-point t_1, with the center point v sitting within a search neighborhood $n(x)$. Thus, all of these atlas patches form an over-complete dictionary $D(x, t_1) = \{P(I_{t_1}^s(v)) | v \in n(x), s = 1, \ldots, N\}$. Since M_{t_1} and $I_{t_1}^s$ are at the same time-point t_1, the appearances of these image patches are similar. For clarity, we vectorize the reference patch $Q(M_{t_1}(x))$ into a column vector $\vec{b}$. Also, we arrange each atlas patch $P(I_{t_1}^s(v))$ into a column vector $\vec{a}_p$ and then assemble them into a matrix $A = [\vec{a}_p]_{p=1, \ldots, \eta}$, where $p = (v, s)$ is a bivariate index for the particular atlas patch $P(I_{t_1}^s(v))$ and $\eta = N \cdot |n(x)|$ denotes the total number of atlas patches in dictionary D.

Inspired by the power of sparse representation, we further look for a sparse coefficient vector $\vec{w} = [w_p]_{p=1, \ldots, \eta}$ to represent the reference patch $\vec{b}$ by the dictionary matrix A, i.e., $\vec{b} \leftarrow A\vec{w}$, where each element in $\vec{w}$ indicates the contribution of a particular atlas patch $\vec{a}_p$ in representing the reference patch $\vec{b}$. Thus, the estimation of $\vec{w}$ falls to the classic LASSO (Least Absolute Shrinkage and Selection Operator) problem [52]:

$$\operatorname*{argmin}_{\vec{w}} \|\vec{b} - A\vec{w}\|^2 + \lambda \|\vec{w}\|_1, \quad s.\, t. \quad \vec{w} > 0 \tag{1}$$

where λ controls the sparsity of the coefficient vector $\vec{w}$. Here, we specifically use $\widetilde{D}(x, t_1)$ to denote the set of selected image patches in $D(x, t_1)$ with the sparse coefficients $w_p > 0$. Since the tissue type for each $\vec{a}_p$ is known, we can calculate the tissue probability $w.r.t.$ WM, GM, and CSF, respectively. After repeating this procedure for every point in the subject image M_{t_1}, we can obtain tissue probability maps (as shown by the solid-border purple box in Fig. 2) to initialize the level set algorithm for segmenting M_{t_1}.

2.2.2. Level set segmentation

Since the sparse patch-based method does not guarantee smooth segmentation of the infant brain MRI, we use a coupled level set algorithm [34], integrated with the previously extracted tissue probability maps, to obtain more accurate segmentation. Specifically, we employ three level sets, with their zero-level surfaces, respectively, denoting for interfaces of WM/GM, GM/CSF, and CSF/background. The tissue probability maps can be treated as prior knowledge and used in the coupled level set segmentation algorithm for improving segmentation accuracy. The tentative segmentation results of M_{t_1} is shown in the dashed-border purple box in Fig. 2.

2.3. Symmetric feature-based image registration, based on segmented infant images

2.3.1. Predict initial deformation pathway

In the following, we follow the sparse patch-based correspondence detection procedure in [42] to calculate the initial deformation pathway between the subject image and the template image.

After sparse patch matching for each point x as described in Section 2.2, we can also get a small set of its possible correspondences, denoted as $P^* = \{p = (v, s) | w_p > 0\}$, by excluding all $\vec{a}_p$ with $w_p = 0$. Then, we will transfer each candidate $p \in P^*$ from the t_1 time-point domain (belonging to the subject image) to the t_2 time domain (belonging to the template image), by following the learned growth trajectory $\varphi_{t_1 \to t_2}^s$ (from Section 2.1). Thus, we can find the corresponding points of the reference point x in the t_2 time-point domain,
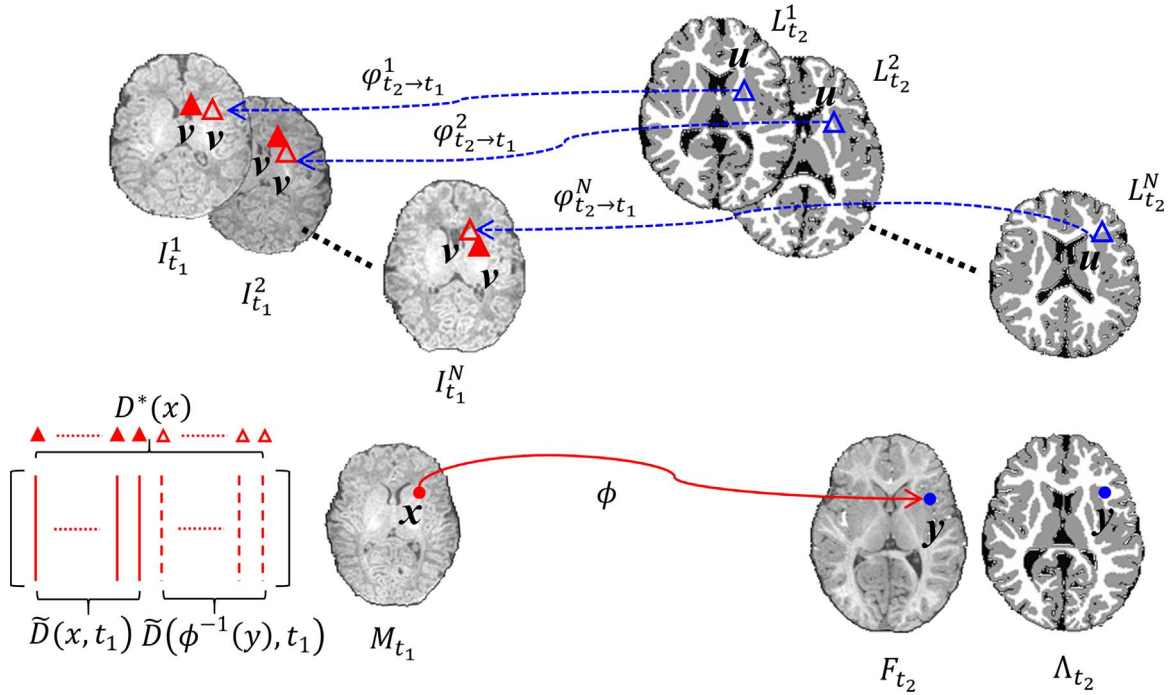
Fig. 4. Construction of the augmented dictionary for joint segmentation and registration. The boost dictionary (bottom left) consist of image patches selected in multi-atlas patch based label fusion (solid lines and solid triangle in $I_{t_1}^s$) and additional image patches (dash lines and dash triangles in $I_{t_1}^s$) which are eventually travelled from the corresponding locations (blue hollow triangles) in template image. Please see the text above for detail. (For interpretation of the references to color in this figure legend, the reader is referred to the web version of this article.)

$U = \{u_p = \varphi_{t_1 \to t_2}^s (v) | p = (v, s) \in P^*\}$. Then, it is not difficult to find the corresponding point y_p in the template image F_{t_2} for each candidate $u_p \in U$, since both y_p and u_p sit in the t_2 time-point domain. After that, we can predict the correspondence for the reference point x by fusing all possible corresponding locations y_p in the template image F_{t_2} w.r.t. the normalized sparse coefficients w_p ($p \in P^*$) estimated in the t_1 time-point domain, i.e., $x \leftrightarrow \sum_{p \in P^*} (w_p \cdot y_p)$. After we visit each point $x \in M_{t_1}$, we can obtain the initial deformation pathway from the template image to the subject image.

2.3.2. Hierarchical symmetric registration approach

Given the segmentation image for the subject image (and also assuming the tissue segmentation of template image is already obtained), we can deploy the state-of-the-art registration method, i.e., symmetric HAMMER [53], to simultaneously estimate the deformation pathways ϕ_1 (from subject image to the hidden common space) and ϕ_2 (from template image to the hidden common space). Since geometric invariant moment (GMI) features are extracted from the segmented images, image registration is free of dynamic appearance changes in the original intensity images. It is worth noting that the deformed subject image w.r.t. ϕ_1 and the deformed template image w.r.t. ϕ_2 should be similar in the end of registration. Importantly, our symmetric image registration can be much more efficient and accurate with the reasonable initial deformation pathways estimated above.

Since ϕ_1 and ϕ_2 are iteratively refined during registration, we use k ($k = 0, ..,K$) to denote the iteration. In the beginning of registration ($k = 0$), $M^{(0)} = M_{t_1}(\phi_1^{(0)})$ and $F^{(0)} = F_{t_2}(\phi_2^{(0)})$, along with the initial deformation pathways $\phi_1^{(0)}$ and $\phi_2^{(0)}$ estimated above. Also, only a small number of key points [53] with distinctive features are selected from $M^{(0)}$ and $F^{(0)}$ to establish anatomical correspondences by matching the GMI features. In the following, we adopt the hierarchical deformation mechanism for establishing the correspondence between the deformed subject image $M^{(k)} = M_{t_1}(\phi_1^{(k)})$ and the deformed template image $F^{(k)} = F_{t_2}(\phi_2^{(k)})$. For each iteration, the key points with distinctive features are selected from $M^{(k)}$ and $F^{(k)}$. The entire deformation pathways $\phi_1^{(k)}$ and $\phi_2^{(k)}$ are steered by the correspondences on these

key points by requiring all other non-key points following the deformations on the nearby key points. With progress of registration, more and more key points are selected to refine the deformation pathways $\phi_1^{(k)}$ and $\phi_2^{(k)}$ regarding to $M^{(k)}$ and $F^{(k)}$, which is repeated until $M^{(k)}$ and $F^{(k)}$ become very similar in the end of registration. Finally, the deformation pathway from template image to subject image can be calculated by $\phi = \phi_1^{(k)} \circ (\phi_2^{(k)})^{-1}$, where '$\circ$' denotes the composition of deformation pathway $\phi_1^{(k)}$ and the inverse deformation pathway $(\phi_2^{(k)})^{-1}$. Vice versa, the reverse deformation pathway ϕ^{-1} can be obtained by $\phi^{-1} = \phi_2^{(k)} \circ (\phi_1^{(k)})^{-1}$.

2.4. Joint segmentation and registration for infant brain images

It is straightforward that better segmentation result can improve the registration accuracy. On the other hand, we argue that refined image registration can further enhance the tissue segmentation result by propagating the reliable label fusion priors from template to subject image domain. Specifically, the key step in tissue segmentation (Section 2.2) is to find correct atlas patches to vote for the tissue type at each point $x \in M_{t_1}$, where the influence of each atlas patch is quantitatively measured by the sparse coefficient w (in Eq. (1)). Due to huge variations across individual subjects and low image contrast in M_{t_1}, however, it is still challenging to obtain optimal sparse coefficient for label fusion, if barely based on intensity image patches. In [54], more accurate label fusion results have been achieved by optimizing the sparse coefficients in the label image domain since the eventual goal of label fusion is to find optimal weights for voting the tissue type, not the representation of intensity image patch. It enlightens us to take advantage of accurate tissue segmentation on the template image by transferring more reliable label fusion priors obtained at each template image point to the corresponding subject image point x. As a result, the tissue segmentation result on subject image M_{t_1} can be gradually improved as the correspondences between M_{t_1} and F_{t_2} become more and more accurate. The procedure of iteratively improving tissue segmentation on M_{t_1} is detailed as follows.

For each point x (red dot in Fig. 4) in the subject image M_{t_1}, we can obtain the corresponding location $y = x + \phi(x)$ ($y \in F_{t_2}$) (blue dot in Fig. 4) in the template image domain, based on the tentatively estimated deformation pathway ϕ (estimated by symmetric image registration in Section 2.3), delineated as a red curve in the bottom of Fig. 4. Then, we regard the label image patch $Q(\Lambda_{t_2}(y))$ extracted at y as the reference patch and deploy the multi-atlas sparse patch representation where the dictionary $D(y,t_2) = \{P(L_{t_2}^s(u))|u \in n(y), n(y) \subset F_{t_2}\}$ consists of the label image patches, falling in the search neighborhood $n(y)$, from all training infant images at t_2 (one year old) time point. After sparse patch representation, we can obtain a sparse coefficient vector with each element $w(s, u)$ suggesting the influence of atlas patch $P(L_{t_2}^s(u))$ in label fusion. Since large value of the sparse coefficient $w(s, u)$ indicates the point y has more likelihood bearing the same tissue type as the underlying atlas patch $P(L_{t_2}^s(u))$, we can pick up a set of atlas patches in the label dictionary $D(y,t_2)$ with sparse coefficient greater than zero. Intuitively, the local anatomy at point y can be represented by the linear combination of selected atlas patches, denoted as $\widetilde{D}(y,t_2) = \{P(L_{t_2}^s(u))|w(s, u) > 0\}$ (illustrated by blue triangles in Fig. 4). It is worth noting that selection of $\widetilde{D}(y,t_2)$ is based on segmented images which is more reliable than estimating based on intensity images [54]. Since the subject point x is the corresponding point of the template point y, such useful information is a very valuable supplement to the initial dictionary $D(x,t_1)$ in label fusion. To transfer $\widetilde{D}(y,t_2)$ to the t_1 time domain, we allow each atlas patch $P(L_{t_2}^s(u))$ in $\widetilde{D}(y,t_2)$ travel from t_2 to t_1 via the previously estimated growth trajectory $\varphi_{t_2 \to t_1}^s$ (blue dash curves in Fig. 4), and provide a set of additional atlas patches, denoted by $\widetilde{D}(\phi^{-1}(y), t_1) = \{P(I_{t_1}^s(v))|w(s, u) > 0, v = u + \varphi_{t_2 \to t_1}^s(u), v \in M_{t_1}, u \in F_{t_2}\}$ (red hollow triangles in Fig. 4), to take part in the tissue segmentation at x. It is worth noting that **(1)** u and v are a pair of temporal correspondence of subject s linked by the growth trajectory $\varphi_{t_2 \to t_1}^s$; **(2)** we extract the intensity image patch at v from the intensity image $I_{t_1}^s$, instead of label image $L_{t_1}^s$.

After that, we can construct the boosted dictionary $D^*(x)$ for point x, which now includes **(1)** $\widetilde{D}(x,t_1)$: a set of selected image patches (solid red triangles in Fig. 4) from the initial dictionary by sparse representation; **(2)** $\widetilde{D}(\phi^{-1}(y), t_1)$: a set of additional image patches (hollow red triangles in Fig. 4) in the t_1 time domain where their corresponding label image patches in the t_2 time domain can well represent the label image patch at location y in the template image. Since the additional image patches are more specific to the point x than the training image patches from the atlases, the augmented dictionary can provide more useful information to guide the tissue segmentation. Using the booted dictionary $D^*(x)$, we can apply sparse patch-based label fusion method to achieve a better segmentation of the subject image M_{t_1}. By alternating these segmentation and registration steps, we can iteratively refine both segmentation and registration results for M_{t_1}.

2.5. Solution for any pair of new infant images in the first year of life

In this section, we provide the solution to extend our joint segmentation and registration framework to any pair of infant images in the first year of life with the possible large age gap. Since the template image plays an important role in guiding the tissue segmentation of new infant image earlier than one year old, we keep using the template image as the bridge to link the joint segmentation and registration for two new infant images. Specifically, our solution has two steps.

1. We first deploy our joint segmentation and registration framework between each new infant image and the template image separately. After converging, we can obtain the segmented image for both new infant images and the deformation pathway from each new infant image toward the template image.

2. Based on the segmented images and the initial deformation pathway, we can directly register the two new infant images by deploying the symmetric registration method. To improve the registration efficiency, we can further combine two deformation pathways obtained in Step 1 into a complete deformation pathway from one infant image to another and used it as the initialization to speed up the registration between two new infant images.

3. Experiments

In total, we collect 10 infant subjects with complete longitudinal data as the training subjects, where each subject has T1- and T2-weighted images at 2 weeks, 3 months, 6 months, 9 months, and 1 year of age. All images were acquired from a Siemens head-only 3T MR scanner. T1-weighted images were acquired with 144 sagittal slices at resolution of $1 \times 1 \times 1 mm^3$. T2-weighted images with 64 axial slices were obtained at resolution of $1.25 \times 1.25 \times 1.95 mm^3$. For each subject, the T2-weighted image is aligned to the T1-weighted image at the same time-point and then further resampled to $1 \times 1 \times 1 mm^3$.

Firstly, we apply our joint segmentation and registration method to align subject of 2-week-old, 3-month-old and 6-month-old to the 1-year-old infant template image (bottom right of Fig. 2). It is noted that the segmented results of 2-weeks-old and 3-month-old images are applied on T2-weighted images, whereas the segmentation of 6-month-old image is applied on T1-weighted images, by choosing the best image contrast of brain tissue at respective time points. To evaluate the segmentation and registration performance, we performed leave-two-subjects-out strategy, where two subjects are randomly chosen from the ten subjects and used as template and subject images, and the other 8 subjects are used as the training images. For all the experiment, the patch size is fixed to $3 \times 3 \times 3\ mm^3$. The search neighborhood in constructing the sparse representation dictionary is fixed to $5 \times 5 \times 5$. Parameter λ in Eq. (1) is empirically fixed to 5.

3.1. Evaluation of segmentation results

For each testing infant image, we have the manual segmentation results of WM, GM, and CSF. Here, we use Dice ratio to quantitatively measure the overlap degree between manual segmentations (used as ground truth) and our estimated tissue segmentations. The sparse patch-based level set segmentation algorithm (without improvement by registration) is used as the baseline method for comparison. The Dice ratios on each tissue type for 2-week-old, 3-month-old and 6-month-old infant brain images are listed in Table 1, Table 2 and Table 3 respectively. After joint segmentation and registration, our method achieves overall 3.0%, 2.1% and 0.7% improvement in segmenting 2-week-old, 3-month-old and 6-month-old infant brain images, respectively. After paired t-test, the improvements in each tissue type are statistically significant. Some typical improvements on 2-week-old and 3-month-old infant brain images are displayed in Fig. 5. It is clear that the initial mis-segmentations (in the left column of Fig. 5) have been successfully corrected based on more and more accurate image registration (in the middle column of Fig. 5).

Table 1

The mean and standard deviation of Dice ratios of WM, GM, and CSF on ten subjects between the 1-year-old manual segmentation and the estimated segmentation from *2-week-old* infant brain image.

	WM (%)	GM (%)	CSF (%)	Overall (%)
Sparse-Level Set	84.5 ± 1.3	85.2 ± 0.9	76.9 ± 2.7	82.2 ± 0.9
Our method	**87.0 ± 0.8**[a]	**86.5 ± 0.6**[a]	**82.0 ± 2.9**[a]	**85.2 ± 1.1**[a]

[a] $p < 0.001$.

Table 2

The mean and standard deviation of Dice ratios of WM, GM, and CSF on ten subjects between the 1-year-old manual segmentation and the estimated segmentation from *3-month-old* infant brain image.

	WM (%)	GM (%)	CSF (%)	Overall (%)
Sparse-Level Set	73.5 ± 7.8	80.1 ± 3.8	79.3 ± 11.5	77.6 ± 7.7
Our method	**77.2 ± 10.1**[a]	**82.0 ± 4.9**[a]	**79.8 ± 11.7**[a]	**79.7 ± 8.9**[a]

[a] $p < 0.005$.

Table 3

The mean and standard deviation of Dice ratios of WM, GM, and CSF on ten subjects between the 1-year-old manual segmentation and the estimated segmentation from *6-month-old* infant brain image.

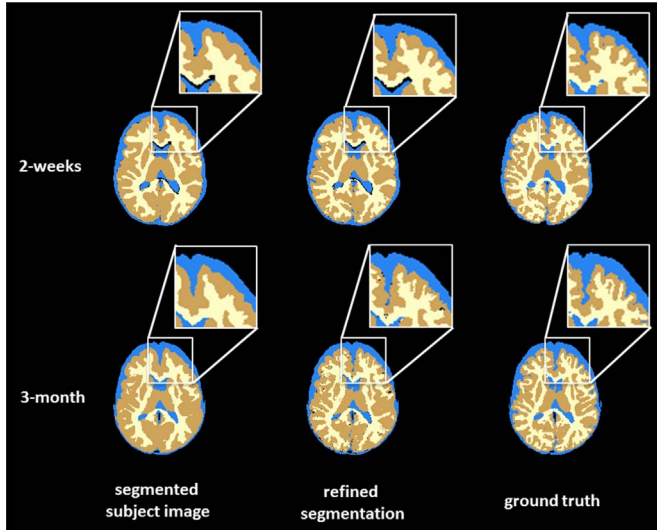|	WM (%)	GM (%)	CSF (%)	Overall (%)
Sparse-Level Set	78.6 ± 2.5	84.3 ± 1.2	75.1 ± 1.9	79.3 ± 1.3
Our method	**81.0 ± 2.8**[a]	**84.6 ± 1.7**	**74.3 ± 1.9**[a]	**80.0 ± 1.7**[a]

[a] $p < 0.05$.

Fig. 5. Segmentation improvements on a 2-week-old infant image and on a 3-month-old infant brain images.

Table 4

Registration results comparison between our proposed method and the state of art methods. The mean and standard deviation of the combined GM and WM Dice ratio, acquired from registering 2-week-old, 3-month-old, 6-month-old to the 1-year-old image, using five different methods.

	2-week to 1-year (%)	3-month to 1-year (%)	6-month to 1-year (%)
MI-method	70.9 ± 2.8	69.4 ± 3.0	79.9 ± 2.9
CC-method	71.4 ± 2.5	68.7 ± 3.1	79.7 ± 2.8
3D-HAMMER	76.4 ± 2.7	75.6 ± 2.8	80.6 ± 2.4
HSR method	77.4 ± 1.5	77.8 ± 1.8	81.8 ± 1.6
Our method	**82.0 ± 1.9**[a]	**83.7 ± 1.7**[a]	**84.5 ± 2.3**[a]

[a] $p < 0.001$.

3.2. Evaluation on registration results

To quantitatively evaluate the registration accuracy of our proposed method to the state-of-the-art deformable image registration methods, we calculated the tissue overlap ratio by deforming the segmented results from 2-weeks-old, 3-month-old, and 6-month-old to the 1-year-old domain. Table 4 shows the mean and standard deviation of the combined GM and WM Dice ratio of the registered images using

Table 5

Registration result comparison between our proposed method and demons registration on intensity images. The mean and standard deviation of the combined GM and WM Dice ratio, acquired from registering between any two time-point images of 2-week-old, 3-month-old and 6-month-old.

	2-week to 3-month (%)	2-week to 6-month (%)	3-month to 6-month (%)
Demons	68.9 ± 9.6	52.7 ± 5.9	49.5 ± 8.3
Our method	**75.7 ± 7.0**[a]	**78.5 ± 2.9**[a]	**78.0 ± 3.0**[a]

[a] $p < 0.001$.

different registration methods, including demons registration method [35], mutual information method (MI-method) [36,37], cross correlation method (CC-method) [38,39], 3D-HAMMER method [40], and our recently proposed learning-based infant image registration method (HSR method) [42]. In registering 2-week-old, 3-month-old, and 6-month-old infant images to the 1-year-old template image, our proposed method achieves highest registration accuracy in terms of Dice ratio. Compared to the best counterpart method (HSR method), the improvements of combined GM and WM Dice ratio are 4.6% for 2-week-old images, 5.9% for 3-month-old images, and 2.7% for 6-month-old images, respectively.

In addition, the mean and standard deviation of the combined GM and WM Dice ratio, by registering any two infant images randomly selected from the 2-week-old, 3-month-old, and 6-month-old cohort are reported in Table 5. Compared to the demons registration method [35] that directly align the infant images based on their intensity images, our method significantly improves the accuracy of the registration in terms of the dice ratio, increasing on average about 6.8%, 25.8% and 28.5% in registering the 2-week-old images to 3-month-old images, 2-week-old images to 6-month-old images, and 3-month-old images to 6-month-old images respectively.

4. Conclusion and future work

In this paper, we propose a novel joint segmentation and registration method for infant brain images by using the growth trajectories learned from a large number of training subjects with complete longitudinal data. Specifically, image segmentation assists the registration by providing accurate tissue segmentations, which avoid the challenge of directly registering the two infant brain images with large appearance changes. In return, the refined image registration can bring more useful information to provide better tissue probability maps for guiding the level set based segmentation. Our reported results showed significant improvement in terms of segmentation and registration accuracy compared to the baseline method.

Currently, due to the lack of longitudinal infant imaging data and the manual segmentation, our method only use 10 longitudinal subjects to form the dictionary. To improve the robustness and accuracy of segmentation and registration, more atlas images with manual segmentation will be added to augment the power of sparse dictionary learning. Meanwhile, our current implementation is mixed with Matlab and C++, which does not fully utilize the multi-core parallel capacity in modern PC. Currently, the computation time for a typical infant image ($256 \times 256 \times 256$ with $1 \times 1 \times 1 mm^3$ image resolution) is a little over two hours. In our future work, we will optimize the code and reduce the computation time to within an hour using OpenMP. Also, we will package our infant joint segmentation and registration method and release to NITRIC (http://nitrc.org/).

Acknowledgement

References

[1] C.R. Almli, M.J. Rivkin, R.C. McKinstry, B.D.C. GroupThe NIH MRI study of normal brain development (Objective-2): newborns, infant, toddlers, and pre-schools, , Neuroimage 35 (2007) 308–325.

[2] W. Gao, H. Zhu, K.S. Giovanello, J.K. Smith, D. Shen, J.H. Gilmore, W. Lin, Emergence of the brain's default network: evidence from two-week-old to 2-year-old healthy pediatric subjects, PNAS 106 (2009) 6790–6795.

[3] J.H. Gilmore, F. Shi, S.L. Woolson, R.C. Knickmeyer, S.J. Short, W. Lin, H. Zhu, D. Shen, Longitudinal development of cortical and subcortical gray matter from birth to 2 years, Cereb. Cortex 22 (2012) 2478–2485.

[4] R. Knickmeyer, S. Gouttard, C. Kang, D. Evans, K. Wilber, J. Smith, R. Hamer, W. Lin, G. Gerig, J. Gilmore, A structural MRI study of human brain development from birth to 2 years, J. Neurosci. 28 (2008) 12176–12182.

[5] H. Hazlett, M. Poe, G. Gerig, R. Smith, J. Provenzale, A. Ross, J. Gilmore, J. Piven, Magnetic resonance imaging and head circumference study of brain size in autism: birth through age 2 years, Arch. Gen. Psychiatry 62 (2005) 1366–1376.

[6] D. Amaral, C. Schumann, C. Nordahl, Neuroanatomy of autism, Trends Neurosci. 31 (2008) 137–145.

[7] S. Zhou, J. Wang, S. Zhang, Y. Liang, Y. Gong, Active contour model based on local and global intensity information for medical image segmentation, Neurocomputing 186 (2016) 107–118.

[8] Z. Ji, Y. Xia, Q. Sun, Q. Chen, D. Feng, Adaptive scale fuzzy local Gaussian mixture model for brain MR image segmentation, Neurocomputing 134 (2014) 60–69.

[9] S. Zhang, Y. Zhan, M. Dewan, J. Huang, D.N. Metaxas, X.S. Zhou, Towards robust and effective shape modeling: sparse shape composition, Med. Image Anal. 16 (2012) 265–277.

[10] S. Zhang, Y. Zhan, D. Metaxas, Deformable segmentation via sparse representation and dictionary learning, Med. Image Anal. 16 (2012) 1385–1396.

[11] S. Zhang, Y. Zhan, M. Dewan, J. Huang, D.N. Metaxas, X.S. Zhou, Deformable segmentation via sparse shape representation, in: G. Fichtinger, A. Martel, T. Peters (Eds.), Medical Image Computing and Computer-Assisted Intervention – MICCAI 2011: 14th International Conference, Toronto, Canada, September 18-22, 2011, Proceedings, Part II, Springer, Berlin, Heidelberg, 2011, pp. 451–458.

[12] T. Wan, B.N. Bloch, S. Danish, A. Madabhushi, A learning based fiducial-driven registration scheme for evaluating laser ablation changes in neurological disorders, Neurocomputing 144 (2014) 24–37.

[13] L. Wang, C. Pan, Nonrigid medical image registration with locally linear recon-struction, Neurocomputing 145 (2014) 303–315.

[14] G. Li, J. Nie, L. Wang, F. Shi, A. Lyall, W. Lin, J. Gilmore, D. Shen, Mapping longitudinal hemispheric structural asymmetries of the human Cerebral Cortex from birth to 2 years of age, Cereb. Cortex 24 (2013) 1289–1300.

[15] J. Nie, G. Li, D. Shen, Development of cortical anatomical properties from early childhood to early adulthood, Neuroimage 76 (2013) 216–224.

[16] F. Shi, P.-T. Yap, G. Wu, H. Jia, J.H. Gilmore, WeiliLin, D. Shen, Infant brain atlases from neonates to 1- and 2-year-olds, PLoS One 6 (2010) e18746.

[17] I. Isgum, M. Staring, A. Rutten, M. Prokop, M.A. Viergever, B. van Ginneken, Multi-atlas-based segmentation with local decision fusion–application to cardiac and aortic segmentation in CT scans, IEEE Trans. Med Imaging 28 (2009) 1000–1010.

[18] P. Coupé, J.V. Manjón, V. Fonov, J. Pruessner, M. Robles, D.L. Collins, Patch-based segmentation using expert priors: application to hippocampus and ventricle segmentation, NeuroImage 54 (2011) 940–954.

[19] T. Tong, R. Wolz, J.V. Hajnal, D. Rueckert, Segmentation of brain images via sparse patch representation, MICCAI Workshop on Sparsity Techniques in Medical Imaging, Nice, France, 2012

[20] G. Wu, M. Kim, G. Sanroma, Q. Wang, B. Munsell, D. Shen, Hierarchical multi-atlas label fusion with multi-scale feature representation and label-specific patch partition, NeuroImage 106 (2015) 34–46.

[21] D. Zhang, Q. Guo, G. Wu, D. Shen, Sparse patch-based label fusion for multi-atlas segmentation, in: P.-T. Yap, T. Liu, D. Shen, C.-F. Westin, L. Shen (Eds.), Multimodal Brain Image Analysis: Second International Workshop, MBIA 2012, Held in Conjunction with MICCAI 2012, Nice, France, October 1-5, 2012. Proceedings, Springer, Berlin, Heidelberg, 2012, pp. 94–102.

[22] R.C. Knickmeyer, S. Gouttard, C. Kang, D. Evans, K. Wilber, J.K. Smith, R.M. Hamer, W. Lin, G. Gerig, J.H. Gilmore, A structural mri study of human brain development from birth to 2 years, J. Neurosci. 28 (2008) 12176–12182.

[23] L. Wang, F. Shi, G. Li, D. Shen, 4D segmentation of brain MR images with constrained cortical thickness variation, PLoS One 8 (2013) e64207.

[24] L. Wang, F. Shi, P.-T. Yap, J.H. Gilmore, W. Lin, D. Shen, 4D multi-modality tissue segmentation of serial infant images, PLoS One 7 (2012) e44596.

[25] L. Wang, F. Shi, P.-T. Yap, W. Lin, J.H. Gilmore, D. Shen, Longitudinally guided level sets for consistent tissue segmentation of neonates, Hum. Brain Mapp. 34 (2013) 956–972.

[26] K. Pohl, J. Fisher, W.E.L. Grimson, R. Kikinis, W.M. Wells, A. Bayesian, Model for joint segmentation and registration, Neuroimage 31 (2006) 228–239.

[27] Z. Xue, D. Shen, C. Davatzikos, CLASSIC: consistent longitudinal alignment and segmentation for serial image computing, in: G.E. Christensen, M. Sonka (Eds.), Information Processing in Medical Imaging, Springer, Glenwood Spring, Colorado, 2005, pp. 101–113.

[28] Z. Xue, D. Shen, C. Davatzikos, CLASSIC: consistent longitudinal alignment and segmentation for serial image computing, Neuroimage 30 (2006) 388–399.

[29] A. Yezzi, L. Zollei, T. Kapur, A variational framework for joint segmentation and registration, IEEE Workshop on Mathematical Methods in Biomedical Image Analysis, 2001, pp. 44–51

[30] A. Gooya, K.M. Pohl, M. Bilello, G. Biros, C. Davatzikos, Joint segmentation and deformable registration of brain scans guided by a tumor growth model, in: G. Fichtinger, A. Martel, T. Peters (Eds.), Medical Image Computing and Computer-Assisted Intervention – MICCAI 2011: 14th International Conference, Toronto, Canada, September 18–22, 2011, Proceedings, Part II, Springer, Berlin, Heidelberg, 2011, pp. 532–540.

[31] M. Miller, A. Banerjee, G. Christensen, S. Joshi, N. Khaneja, U. Grenander, L. Matejic, Statistical methods in computational anatomy, Stat. Methods Med. Res. 6 (1997) 267–299.

[32] P. Thompson, A. Toga, A framework for computational anatomy, Comput. Vis. Sci. 5 (2002) 13–34.

[33] P.M. Thompson, J.N. Giedd, R.P. Woods, D. MacDonald, A.C. Evans, A.W. Toga, Growth patterns in the developing brain detected by using continuum mechanical tensor maps, Nature 404 (2000) 190–193.

[34] L. Wang, F. Shi, G. Li, Y. Gao, W. Lin, J.H. Gilmore, D. Shen, Segmentation of neonatal brain MR images using patch-driven level sets, Neuroimage 84 (2014) 141–158.

[35] T. Vereauteren, X. Pennec, A. Perchant, N. Ayache, Non-parametric diffeomorphic image registration with the demons algorithm, Medical Image Computing and Computer-Assisted Intervention- MICCAI 2007, Pt 2, Proceedings, 4792 (2007) 319-326

[36] F. Maes, A. Collignon, D. Vandermeulen, G. Marchal, P. Suetens, Multimodality image registration by maximization of mutual information, IEEE Trans. Med. Imaging 16 (1997) 187–198.

[37] W.M. Wells 3rd, P. Viola, H. Atsumi, S. Nakajima, R. Kikinis, Multi-modal volume registration by maximization of mutual information, Med Image Anal. 1 (1996) 35–51.

[38] W.K. Pratt, Correlation techniques of image registration, IEEE Trans. Aerosp. Electron. Syst. AES-10 (1974) 353–358.

[39] A. Roche, G. Malandain, X. Pennec, N. Ayache, The correlation ratio as a new similarity measure for multimodal image registration, in: W.M. Wells, A. Colchester, S. Delp (Eds.), Medical Image Computing and Computer-Assisted *Intervention — MICCAI'98*: First International Conference Cambridge, MA, USA, October 11–13, 1998 Proceedings, Springer, Berlin, Heidelberg, 1998, pp. 1115–1124.

[40] S. Dinggang, C. Davatzikos, HAMMER: hierarchical attribute matching mechanism for elastic registration, IEEE Trans. Med. Imaging 21 (2002) 1421–1439.

[41] Y.K. Dai, F. Shi, L. Wang, G.R. Wu, D.G. Shen, iBEAT: a toolbox for infant brain magnetic resonance image processing, Neuroinformatics 11 (2013) 211–225.

[42] Y. Wu, G. Wu, L. Wang, B. Munsell, Q. Wang, W. Lin, Q. Feng, W. Chen, D. Shen, Hierarchical and symmetric infant image registration by robust longitudinal-example-guided correspondence detection, Med. Phys. 42 (2015) 4174–4189.

[43] F. Shi, Y. Fan, S. Tang, J.H. Gilmore, W. Lin, D. Shen, Neonatal brain image segmentation in longitudinal MRI studies, Neuroimage 49 (2010) 391–400.

[44] F. Shi, D. Shen, P.-T. Yap, Y. Fan, J. Cheng, H. An, L.L. Wald, G. Gerig, J.H. Gilmore, W. Lin, CENTS: cortical enhanced neonatal tissue segmentation, Hum. Brain Mapp. 32 (2011) 382–396.

[45] G. Wu, Q. Wang, H. Jia, D. Shen, Registration of longitudinal image sequences with implicit template and spatial-temporal heuristics, in: T. Jiang, N. Navab, J.P.W. Pluim, M.A. Viergever (Eds.), Medical Image Computing and Computer-Assisted Intervention – MICCAI 2010: 13th International Conference, Beijing, China, September 20–24, 2010, Proceedings, Part II, Springer, Berlin, Heidelberg, 2010, pp. 618–625.

[46] G. Wu, Q. Wang, D. Shen, Registration of longitudinal brain image sequences with implicit template and spatial–temporal heuristics, NeuroImage 59 (2012) 404–421.

[47] D. Shen, C. Davatzikos, HAMMER: hierarchical attribute matching mechanism for elastic registration, IEEE Trans. Med. Imaging 21 (2002) 1421–1439.

[48] F.L. Bookstein, Principal warps: thin-plate splines and the decomposition of deformations, IEEE Trans. Pattern Anal. Mach. Intell. 11 (1989) 567–585.

[49] H. Chui, A. Rangarajan, A new point matching algorithm for non-rigid registration, Comput. Vis. Image Underst. 89 (2003) 114–141.

[50] G. Wu, H. Jia, Q. Wang, D. Shen, SharpMean: groupwise registration guided by sharp mean image and tree-based registration, NeuroImage 56 (2011) 1968–1981.

[51] J. Ashburner, A fast diffeomorphic image registration algorithm, NeuroImage 38 (2007) 95–113.

[52] R. Tibshirani, Regression shrinkage and selection via the lasso, J. R. Stat. Soc.: Ser. B (Stat. Methodol.) 58 (1996) 267–288.

[53] G. Wu, M. Kim, Q. Wang, D. Shen, S-HAMMER: hierarchical attribute-guided, symmetric diffeomorphic registration for MR brain images, Hum. Brain Mapp. (2013).

[54] Y. Song, G. Wu, Q. Sun, K. Bahrami, C. Li, D. Shen, Progressive label fusion framework for multi-atlas segmentation by dictionary evolution, in: N. Navab, J. Hornegger, M.W. Wells, F.A. Frangi (Eds.), Medical Image Computing and Computer-Assisted Intervention – MICCAI 2015: 18th International Conference, Munich, Germany, October 5–9, 2015, Proceedings, Part III, Springer International Publishing, Cham, 2015, pp. 190–197.

Pei Dong is a Postdoctoral Fellow at the University of North Carolina at Chapel Hill, USA. He received his B.S and M.S. degree in biomedical engineering from the Southeast University, China, and a Ph.D. degree in biomedical engineering from INSA-Lyon, France. His main research interests include image segmentation, registration and quantification methods to the biomedical applications. His current research interests mainly focus on image segmentation, image registration and the application to the infant brain development and diseases.

Dinggang Shen was a Tenure-Track Assistant Professor with the University of Pennsylvania and a Faculty Member with the Johns Hopkins University. He is currently a Professor of radiology, computer science, and biomedical engineering with the Department of Radiology and the Biomedical Research Imaging Center (BRIC), The University of North Carolina, Chapel Hill. He is also the Director of the Image Display, Enhancement, and Analysis Laboratory in the Department of Radiology and of the medical image analysis core in the BRIC. He has published more than 300 papers in international journals and conference proceedings. His research interests include medical image analysis, computer vision, and pattern recognition. Prof. Shen serves as an Editorial Board Member for four international journals.

Li Wang is a Research Instructor from the University of North Carolina at Chapel Hill, USA. He works with Professor Dinggang Shen in Medical Image Analysis field. His research interests focus on image segmentation, image registration, cortical surface analysis, machine learning and their applications to normal early brain development and disorders. His current focus is on the neonatal brain image segmentation and serial infant brain images.

Guorong Wu received the Ph.D. degree in computer science and engineering from Shanghai Jiao Tong University, Shanghai, China. He is currently with the Image Display, Enhancement, and Analysis Research Laboratory, The University of North Carolina, Chapel Hill, as an Assistant Professor. His research interests focus on the fast and robust analysis of large population data, computer assisted diagnosis, and image-guided radiation therapy.
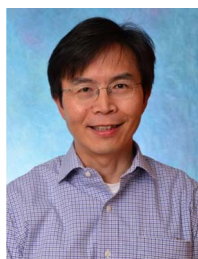
Weili Lin is currently the Director of the Biomedical Research Imaging Center (BRIC), The University of North Carolina, Chapel Hill. His research interests include PET and MR imaging, and their applications to cerebral ischemia and human brain development.